Int. J. Heat Mass Transfer. Vol. 29, No. 6, pp. 831–839, 1986
Printed in Great Britain

0017–9310/86 $3.00 + 0.00
Pergamon Journals Ltd.

Heat transfer from rotating annular fins

E. M. SPARROW and C. S. PRESTON
Department of Mechanical Engineering, University of Minnesota, Minneapolis, MN 55455, U.S.A.

(*Received* 18 *September* 1985 *and in final form* 20 *December* 1985)

Abstract—Experiments have been performed to determine the heat transfer coefficients for arrays of shaft-attached, rotating annular fins. The experiments encompassed a wide range of rotational speeds and interfin spacings (including the limiting case of the single annular fin). The efficiency of the fins was equal to one. It was found that the fin heat transfer coefficient decreased with decreasing interfin spacing, the extent of the decrease being of major proportions at low rotational speeds but being quite moderate at high speeds. Thus, closely spaced fins can be used at high rotational speeds without a significant spacing-related decrease in the transfer coefficient, but at low speeds the fins must be farther apart to avoid overly low values of the coefficient. The heat transfer coefficient also decreased as the rotational speed decreased, with a particularly rapid dropoff at low speeds when the interfin spacing was small. For the most part, the fin heat transfer coefficients substantially exceeded those for an unfinned rotating shaft, thereby providing an incentive for finning. It was also found that at high rotational speeds, the heat transfer coefficient for a rotating disk served as a lower bound for the annular-fin heat transfer coefficients. To facilitate the use of the results for design, a correlation was developed which represents the fin heat transfer coefficient as a continuous function of the investigated independent parameters.

INTRODUCTION

THE USE of fins to enhance convective heat transfer is standard practice in a broad range of technologies. A major issue in the design of fins is the availability of heat transfer coefficients which are appropriate to the type of fluid flow which passes over the fins. In reality, the fluid flows induced by the presence of fins are often highly complex, so that available coefficients tend to be no more than estimates. In certain situations, the necessary heat transfer coefficients are altogether unavailable, and it is such a situation that is the focus of the present work.

Consideration is given here to an array of annular fins affixed to a rotating shaft. Such fins may be used to increase the rate of heat transfer from the shaft to the surrounding fluid. The fluid motions are induced solely by the rotation of the shaft and are, therefore, primarily circumferential. This distinctive pattern of fluid flow sets the rotating annular-fin array apart from more familiar annular-fin configurations, which are stationary and are washed by crossflows.

A survey of the heat transfer literature failed to disclose prior work on the heat transfer characteristics of shaft-attached, rotating annular fins, despite numerous studies involving other types of rotating surfaces (e.g. [1]). Among the latter, the most closely related to the annular-fin array are the rotating disk and the unfinned, rotating shaft. Indeed, in the absence of annular-fin data, it is likely that the available data for the disk and the unfinned shaft would be used to guide the design of the fins. The present annular-fin data will be compared with literature information for the disk and the shaft. Although the fluid flows for the three configurations are strongly circumferential, there are major differences in other aspects of the respective flow patterns, which should be reflected in the heat transfer characteristics.

The work described here encompassed a systematic set of experiments in which primary attention was focused on the effects of interfin spacing and rotational speed on the per-fin heat transfer coefficient. The investigated spacings included the entire practical range as well as the limiting case of a single annular fin (i.e. infinite interfin spacing), while the rotational speed was varied by nearly an order of magnitude. For the sake of generality, the experiments were conducted with fins whose efficiency is equal to one (i.e. isothermal fins). To avoid end effects in the heat transfer results, arrays consisting of either eight or 10 annular fins were employed (except, of course, for the single-fin case), with the heat transfer measurements made at the centralmost pair of fins. Supplementary experiments were performed to examine the possible intrusive effects of natural convection.

In the presentation of the data, a universal correlation was developed which relates the Nusselt number to the dimensionless interfin spacing and to the rotational Reynolds number.

THE EXPERIMENTS

The fin heat transfer coefficients were determined by applying the analogy between heat and mass transfer to mass transfer measurements made with the naphthalene sublimation technique. In general, the naphthalene technique affords higher measurement accuracy, smaller extraneous losses, and simpler fabrication than do corresponding heat transfer experiments. In particular, for the physical situation to be investigated here, the use of the mass transfer

NOMENCLATURE

A	mass transfer surface area of a fin
D_i	inner diameter of annular fin
D_o	outer diameter of annular fin
$\mathscr{D}$	mass diffusion coefficient
K	fin mass transfer coefficient, equation (1)
$\dot{M}$	rate of mass transfer per fin
R_i	inner radius of annular fin
R_o	outer radius of annular fin
R^*	radius for characteristic velocity, equation (5)
Re_i	Reynolds number, $(R_i\omega)D_i/\nu$
Re_s	Reynolds number, $(R_i\omega)S/\nu$
Re^*	Reynolds number, $(R^*\omega)S/\nu$
S	interfin spacing
Sc	Schmidt number
Sh_i	fin Sherwood number, $KD_i/\mathscr{D}$
Sh_s	fin Sherwood number, $KS/\mathscr{D}$
V	characteristic velocity.

Greek symbols

λ	function of S/R_i in definition of R^*, equation (5)
ν	kinematic viscosity
ρ_{nw}	naphthalene vapor density at fin surface
$\rho_{n\infty}$	naphthalene vapor density in ambient
ω	angular velocity.

technique avoids the difficulties of conveying electric power and thermocouple e.m.f.s across a rotating interface.

Another advantage stems from the nature of the boundary condition at the subliming naphthalene surface. That condition, uniform naphthalene vapor density, corresponds to uniform surface temperature in the analogous heat transfer problem. Therefore, the heat transfer coefficients deduced from the mass transfer measurements correspond to isothermal fins. This feature avoids the need to correct for the effect of the fin temperature drop, as is common in the processing of data from fin-related heat transfer experiments. Such corrections (based on the fin efficiency) are, in themselves, of uncertain accuracy, so that the accuracy of the corrected heat transfer coefficients is also uncertain.

Experimental apparatus

A schematic diagram of the experimental apparatus is presented in Fig. 1. The main components of the apparatus included: (a) an array of annular fins, (b) spacer rings which established the interfin spacing, (c) a shaft over which the fins and rings were slipped, (d) an end cap which fixed the fin-spacer assembly in place, and (e) a holder which supported the shaft and interfaced with the spindle of a vertical milling machine which served as the source of rotation. An enlarged view of a portion of the fin-spacer assembly is provided by Fig. 2.

Each fin was an annular disk with a bore diameter equal to that of the shaft (clearance = 0.00254 cm) and an outer diameter equal to D_o. All the disks were made of brass and had a common thickness of 0.254 cm. As seen in Figs. 1 and 2, two types of fins were used in assembling the array. One type was provided with a naphthalene-filled, annular cavity. The outer wall of the cavity was beveled (Fig. 2) to enable the exposed surface of the naphthalene to extend to the periphery of the fin, aside from a 0.020-cm retaining rim. The sublimation which occurs at the surface of the naphthalene simulates the fin heat loss. In keeping with annular fin practice, this surface will be characterized by its diameter ratio D_o/D_i, which was fixed at 1.55 (D_i = 2.858 cm, D_o = 4.445 cm).

Two of the just-described fins were positioned on the

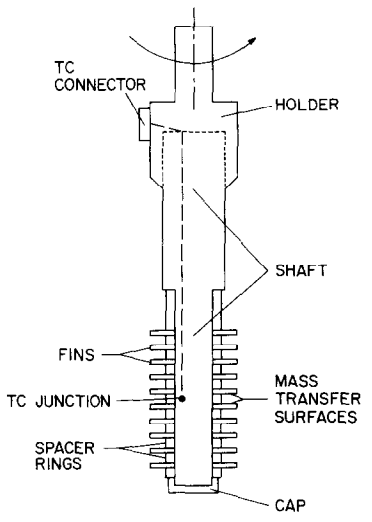

FIG. 1. Schematic diagram of the experimental apparatus.

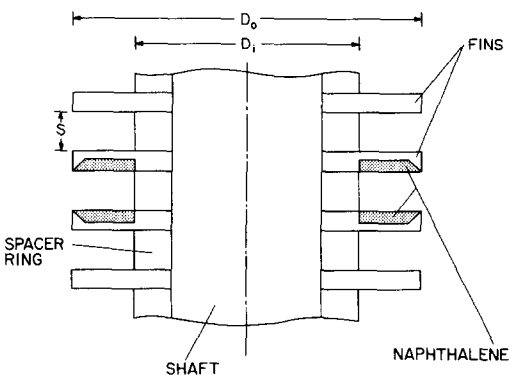

FIG. 2. Representative portion of the fin–spacer assembly.

shaft so that their naphthalene-coated surfaces faced each other. The exposed metallic surfaces of these fins (i.e. the rear face and the tip) did not participate in the mass transfer process.

The other fins in the array were purely metallic (i.e. without naphthalene) and were, therefore, nonparticipants in the mass transfer. Their function was to create a fluid flow pattern in the central portion of the array which closely corresponded to that for an infinite array. The two mass-transfer-active fins were centered in the array, midway between the ends.

Each spacer was an annular ring with a bore diameter equal to that of the shaft and an outer diameter D_i (Fig. 2). The spacers were made of brass. The axial length of the spacer rings served to establish the interfin spacing. Three multi-fin arrays were investigated, respectively characterized by interfin spacings $S/R_i = 0.178$, 0.356, and 0.711 ($S = 0.254$, 0.508, and 1.016 cm). As can be seen in Fig. 1, a supplementary spacer was, when appropriate, put in place atop the uppermost fin in order to tailor the overall length of the array to the length of the working section of the shaft.

The shaft onto which the rings and fins were assembled was made of Delrin, a free-machining plastic. Delrin was chosen as the shaft material to thermally isolate the fin array from the spindle of the milling machine which served as the source of rotation. As seen in Fig. 1, a shoulder (i.e. an abrupt change of diameter) was machined into the shaft to serve as a positive stop for the fin-spacer array. The diameter of the lower portion of the shaft (i.e. the working section) was 1.905 cm, and the other shaft dimensions are to scale in Fig. 1.

For the interfin spacings $S/R_i = 0.178$ and 0.356, 10 fins were used in the array, while for the $S/R_i = 0.711$ spacing, there were eight fins in the array. To model the limiting case of infinite interfin spacing, a single mass-transfer-active fin, centered in the working length of the shaft, was employed along with sufficient spacers to form a continuous surface of diameter D_i both above and below the fin.

With the fins and spacers in place, the working section of the Delrin shaft is, in effect, the *inner* core of a shaft whose outer diameter is defined by the outside surface of the spacers. Thus, from the standpoint of the fluid flow and heat transfer, the diameter of the rotating shaft is D_i.

The assembly of fins and spacers was locked in place by an aluminum cap which fitted over the lower end of the Delrin shaft. The cap exerted upward pressure on the adjacent spacer ring when a retaining screw was tightened.

The upper end of the Delrin shaft mated with a holder which, in turn, mated with the rotating spindle of a vertical milling machine. The holder was made of steel for strength. Collinearity of the axes of the holder and the shaft was ensured by machining them together in a lathe.

During the course of the research, the milling machine was operated at seven fixed rotational speeds between 264 and 2237 r.p.m. These speeds were periodically verified by both a direct-contact and an optical tachometer.

Figure 1 illustrates the presence of a thermocouple that was installed adjacent to the mass-transfer-active fins in order to measure the temperature of the naphthalene. The thermocouple junction and the lead wires were laid in a shallow groove in the Delrin shaft. The groove extended from the junction to the steel holder. It was filled with body putty, after which the surface was sanded smooth. The lead wires which emerged from the groove at its upper end were threaded through a small hole in the holder and terminated in the socket portion of a subminiature, quick-connect connector taped to the side of the holder. During periods of rotation, the thermocouple circuit was not closed; rather, as will be described shortly, the temperature measurement was accomplished after the rotating shaft was brought to rest. The thermocouple was made of 30-gage chromel and constantan wire and was calibrated prior to its installation.

The apparatus illustrated in Figs. 1 and 2 and discussed in the foregoing was supplemented by auxiliary equipment and by instrumentation. To suppress sublimation from the mass-transfer-active fins during certain preparatory stages of a data run, an air-tight shroud was fabricated which totally enveloped the two active fins. Aluminum was chosen for the shroud material because of its high thermal conductivity—a factor which contributed to the more rapid attainment of thermal equilibrium of the shrouded assembly. The storage, transport, and assembly of the active fins and the adjacent spacers was facilitated by the use of a stand consisting of a Delrin shaft (equal in diameter to the rotating shaft) and an integral base. In particular, the active fins and adjacent spacers could be preassembled on the stand and then transferred as a unit to the shaft of the rotational apparatus.

The mass transfer coefficients were determined by measuring the change of mass of the active fins which occurred during a data run. The mass measurements were made with a Sartorius ultra-precision, electronic analytical balance with a resolution of 10^{-5} g and a capacity of 166 g. For the shaft-embedded thermocouple, the e.m.f.s were read with a 1 μV digital voltmeter.

Experimental procedure

The naphthalene face of each mass-transfer-active fin was implanted by a casting procedure. As a first step, the residual naphthalene remaining from the preceding data run was removed by evaporation and melting. Then, the fin was clamped in place on a highly polished, stainless steel plate with the cavity opening facing downward. Molten naphthalene was then poured into the cavity through an aperture in the rear surface of the fin, while the displaced air escaped through a second aperture. Once solidification was completed, the fin was separated from the polished plate, exposing the

cast naphthalene surface, the finish of which was comparable to that of the plate. The pouring and vent apertures were sealed with impermeable tape to prevent sublimation.

The mass transfer rate is proportional to the naphthalene vapor pressure at the surface of the fin. Since the vapor pressure is highly sensitive to temperature (10% change per °C), strict procedures were adopted to attain temperature constancy during the course of a data run. These procedures included lengthy equilibration periods prior to the data run, both in the presence and in the absence of rotation. In particular, the run proper was preceded by a period during which the fully assembled apparatus (with the shroud in place) was rotated at the preselected speed for the run, with temperature measurements being made periodically until a steady value was attained. Then, the shroud was removed and the data run initiated.

Another thermally-related precaution was the avoidance of finger contact with the mass-transfer-active fins, and insulated gloves were worn whenever such contact was necessary. Care was also taken to attain constancy of the laboratory ambient temperature and also to minimize extraneous air currents.

As noted earlier, temperature measurements were not made when the shaft was rotating. To facilitate the temperature measurement, the rotating spindle of the milling machine was braked to an abrupt halt, and the plug portion of the connector was mated with the socket portion. These operations, together with the reading of the thermocouple e.m.f. from the display of the digital voltmeter, were accomplished in about 10 s.

The mass-transfer-active fins were weighed both immediately preceding and immediately following a data run. The duration of the run was selected so that the sublimation-related recession of the fin was no more than 0.0025 cm, which corresponded to a change of mass during the run of about 0.02 g. After the completion of a run, a calibration procedure was performed to determine the extent of the extraneous sublimation which may have occurred during the weighing, setup, and equilibration periods. The resulting correction in the mass transfer ranged from 1 to $1\frac{1}{2}\%$.

RESULTS AND DISCUSSION

Data reduction

The per-fin mass transfer coefficient K was evaluated from the defining equation

$$K = (\dot{M}/A)/(\rho_{nw} - \rho_{n\infty}). \quad (1)$$

In this equation, $\dot{M}$ is the rate of mass transfer and A is the surface area of the naphthalene, both per fin. The numerical values of $\dot{M}$ were calculated from the change of mass which occurred during a data run and from the duration of the run. In the denominator of equation (1), ρ_{nw} and $\rho_{n\infty}$ are, respectively, the naphthalene vapor densities at the fin surface and in the ambient. The former was evaluated from the vapor pressure/temperature relation for naphthalene in conjunction with the perfect gas law, while the latter was zero for the present experiments.

The dimensionless counterpart of the mass transfer coefficient is the Sherwood number Sh, the evaluation of which requires the specification of a characteristic dimension. In what follows, Sherwood number results based on both the interfin spacing S and on the inner diameter D_i of the annular fin will be presented, with the respective definitions,

$$Sh_s = KS/\mathscr{D}, \quad Sh_i = KD_i/\mathscr{D}. \quad (2)$$

The diffusion coefficient $\mathscr{D}$ appearing in equation (2) was eliminated by means of the Schmidt number $Sc = \nu/\mathscr{D}$, with $Sc = 2.5$ and ν as the kinematic viscosity of air. The interfin spacing S was corrected to account for sublimation-related recession of the naphthalene surface.

Another key dimensionless group in the presentation of the results is the Reynolds number, for which a characteristic dimension and a characteristic velocity have to be specified. To match the Sh_s and Sh_i definitions of the Sherwood number, corresponding Reynolds numbers Re_s and Re_i may be defined with S and D_i as the respective characteristic dimension. In view of the different dimensions in Re_s and Re_i, it was deemed appropriate to use the same characteristic velocity in both, for which the rotational speed $R_i\omega$ of the unfinned shaft was selected. Therefore,

$$Re_s = (R_i\omega)S/\nu, \quad Re_i = (R_i\omega)D_i/\nu. \quad (3)$$

In the correlation effort to be detailed later, it was found useful to vary the characteristic velocity as a function of the interfin spacing.

The other variable dimensionless parameter of the work, in addition to Sh and Re, is the ratio S/R_i. The diameter ratio D_o/D_i of the annular fin was fixed at 1.55.

Mass transfer coefficients

The per-fin mass transfer coefficients for all of the investigated rotational speeds and interfin spacings are presented in Fig. 3. In the figure, the Sherwood number Sh_i is plotted as a function of the Reynolds number Re_i for parametric values of the dimensionless interfin spacing S/R_i. Note that both Sh_i and Re_i are based on the characteristic dimension D_i, which was fixed throughout the experiments. In addition, the velocity $R_i\omega$ embedded in Re_i is a direct reflection of ω because of the constancy of R_i ($= \frac{1}{2}D_i$). Thus, although Fig. 3 is couched in dimensionless terms, it is actually a graph showing the variation of the mass transfer coefficient with the rotational speed for several fixed values of the interfin spacing. To provide continuity, smooth curves have been passed through the data for each spacing. Also presented in the figure for comparison purposes are results for other rotating configurations. The comparisons will be dealt with in a later section.

Inspection of Fig. 3 shows that, as expected, the transfer coefficient increases with increasing rotational

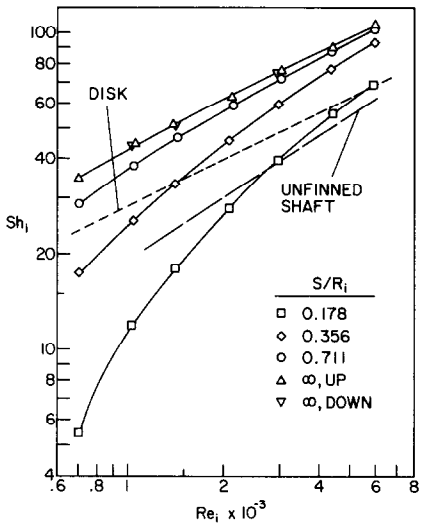

FIG. 3. Dependence of the fin Sherwood number on the Reynolds number for parametric values of the interfin spacing.

speed. However, the sensitivity of the coefficient to changes in speed is strongly dependent on the interfin spacing. In particular, the smaller the spacing, the greater is the sensitivity. Thus, for example, for the smallest spacing ($S/R_i = 0.178$), the transfer coefficient increases by more than a factor of 12 over the investigated range of rotational speeds, while for the largest spacing ($S/R_i = \infty$), the increase is a factor of three.

The aforementioned characteristics are reflected in the shapes of the Sh_i, Re_i curves. For the largest spacing, the curve departs only slightly from a straight line, tending to drop off gradually at lower Re_i. As the spacing decreases, the low-Re dropoff becomes progressively greater, and at the smallest spacing the curve plummets. This behavior is due to the inability of the ambient air to penetrate tight interfin spaces when the rotational speed is low.

Further examination of Fig. 3 shows that at all rotational speeds, the transfer coefficient decreases as the interfin spacing decreases. The change in the transfer coefficient with spacing is enormous at low rotational speeds but moderates as the rotational speed increases. The moderation is due to the relatively rapid rise of the low-spacing transfer coefficient with increasing speed, reflecting the greater ability of the ambient air to penetrate tight interfin spaces. Thus, a $6\frac{1}{2}$-fold increase of Sh_i with increasing spacing (i.e. S/R_i increasing from 0.178 to ∞) at the lowest Reynolds number (700) diminishes to a 50% increase at the highest Reynolds number (6000).

The foregoing findings have direct implications for design. In particular, at high rotational speeds, closely spaced fins can be used without incurring a significant spacing-related decrease in the transfer coefficient. On the other hand, at low speeds, the fins must be spaced farther apart to avoid overly low values of the coefficient.

Attention will now be turned to the two sets of data (upfacing and downfacing triangles) for the infinite-spacing (i.e. single-fin) case. One set was obtained with the mass transfer surface facing upward, while the other set was for the mass transfer surface facing downward. The motivation for employing these two orientations was to investigate the possible effects of natural convection. If such effects existed, they would be more pronounced for the single fin and at lower rotational speeds.

The primary set of data was collected for the upfacing orientation. For the downfacing orientation, experiments were performed at four Reynolds numbers. For $Re_i = 700$, the upfacing and downfacing data are coincident and could not be plotted separately. For the other three cases, the slight Reynolds number displacement enabled the individual points to be plotted, revealing excellent agreement. Another indication of the absence of orientation effects is provided by the fact that in the multiple-fin experiments, the mass transfers at the two active fins generally agreed to within 1–$1\frac{1}{2}$%, without a systematic difference in the mass transfer at the upfacing or downfacing fins.

The possible effects of room air currents were examined by performing data runs in the absence and in the presence of room air conditioning. Although these comparison experiments were carried out for the most disturbance-prone cases—the lowest Reynolds number and the largest interfin spacings—there were no measurable differences in the Sherwood number.

In general, whenever verification runs were made, data repeatability was in the 1% range.

Figure 3 provides mass transfer information for any value of the Reynolds number in the investigated range but is limited to discrete interfin spacings. To provide results which are a continuous function of the spacing, a crossplot of the Sh_i, Re_i curves of Fig. 3 has been made, the end result of which is presented in Fig. 4. In this figure, the Sherwood number Sh_i is plotted as a function of the inverse spacing ratio R_i/S for parametric values of the Reynolds number Re_i. The inverse spacing (rather than the spacing itself) was chosen as the abscissa variable to enable the results for the infinite spacing case to be included in the figure. As already discussed in connection with Fig. 3, Sh_i and Re_i may be respectively regarded as reflecting the mass transfer coefficient and the rotational speed. The discrete points appearing in Fig. 4 are those obtained from the cross-plotting, and smooth curves (i.e. the solid lines) have been passed through the points for continuity. The dashed lines appearing in the figure will be derived and discussed later.

Figure 4 affirms the previously identified decrease of the mass transfer coefficient with decreasing interfin spacing, the extent of the decrease being markedly accentuated at lower Reynolds numbers. The sensitivity of the transfer coefficient to changes in spacing is moderate at large spacings (small R_i/S) and becomes greater as the spacing decreases.

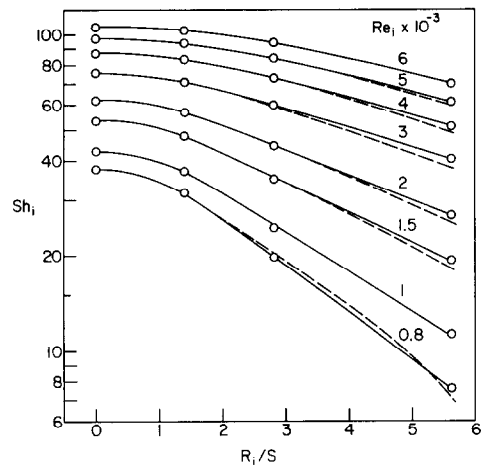

FIG. 4. Dependence of the fin Sherwood number on the interfin spacing for parametric values of the Reynolds number.

Development of a correlation

Both Figs. 3 and 4 share the common characteristic that one of the independent parameters is varied discretely while the other varies continuously. A correlation will now be sought which will represent the Sherwood number as a continuous function of both of the parameters. The correlation will be developed by making use of the freedoms available in selecting the characteristic dimension in Sh and the characteristic dimension and velocity in Re.

As a first step, the interfin spacing S was selected to serve as the characteristic dimension in both Sh and Re while maintaining the characteristic velocity as $R_i\omega$. The resulting Sherwood and Reynolds numbers, Sh_s and Re_s, evaluated for the finite S/R_i data only, are plotted in Fig. 5. From the figure, it is seen that the Sh_s, Re_s distributions for the various S/R_i are distinct (i.e. they have not merged). The distributions are, however, similar in shape, and this suggests that a horizontal translation of any two of the three curves (or of all three) might yield the desired universal curve. Such a translation can be accomplished by a redefinition of the characteristic velocity V which appears in the Reynolds number. To this end, let

$$V = R^*\omega \tag{4}$$

where R^* is related to the radial dimensions R_i and R_o of the annular fin as

$$R^* = R_i + \lambda(R_o - R_i) \tag{5}$$

and λ is an as-yet undetermined function of S/R_i. With this, the Reynolds number can be written as

$$Re^* = (R^*\omega)S/\nu \tag{6}$$

so that

$$Re^*/Re_s = R^*/R_i = 1 + \lambda[(R_o/R_i) - 1]. \tag{7}$$

It remains to be shown that values of $\lambda = \lambda(S/R_i)$ can be found which translate the Sh_s, Re_s curves of Fig. 5 so that they coincide.

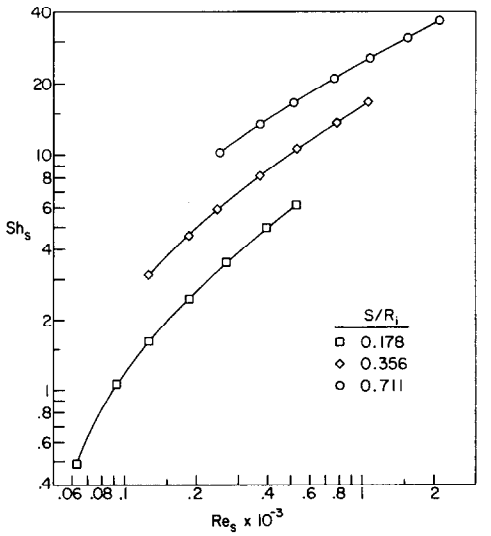

FIG. 5. Rephrasing of the mass transfer results in terms of Sherwood and Reynolds numbers based on the interfin spacing S as the characteristic dimension.

As long as congruence of the curves is achieved, it is immaterial how they are translated. Therefore, the numerical value of λ for one of the three interfin spacings was selected arbitrarily, namely, $\lambda = 1$ for $S/R_i = 0.711$. The λ values for the other S/R_i were found by trial and error. The procedure involved guessing a λ value for a particular S/R_i, computing the Re^* corresponding to the given Re_s from equation (7), and then plotting the Sh_s, Re^* results. The Sh_s, Re^* distributions for the three S/R_i were plotted together and their degree of convergence assessed by visual inspection. Changes were made in the λ values until the three distributions merged into one.

A further test of the quality of the λ determination was to employ the universal Sh_s, Re^* distribution to predict the experimental results given in Fig. 4. Indeed, it was the accuracy of that prediction which ultimately led to the selection of the final values of λ. In this way, the $\lambda(S/R_i)$ values which resulted in a universal Sh_s, Re^* distribution were found to be $\lambda(0.178) = -1.1248$, $\lambda(0.356) = -0.4680$, and $\lambda(0.711) = 1$, the latter by definition. Note that the negative values of λ result in $R^* > R_i$, as does $\lambda = 1$.

It is noteworthy that λ increases with S/R_i and, correspondingly, so does the radius R^* [equation (5)] which fixes the characteristic velocity $V = R^*\omega$. The increase of V with S/R_i reflects the greater ease with which the ambient air can penetrate the interfin space as the spacing is increased.

The universal Sh_s, Re^* distribution is presented in Fig. 6. The actual data points, keyed to their S/R_i values, are shown in the figure to illustrate the fidelity with which the experimental data are represented by the universal curve. Inspection of the figure indicates that all of the data fall on a single curve with virtually no scatter.

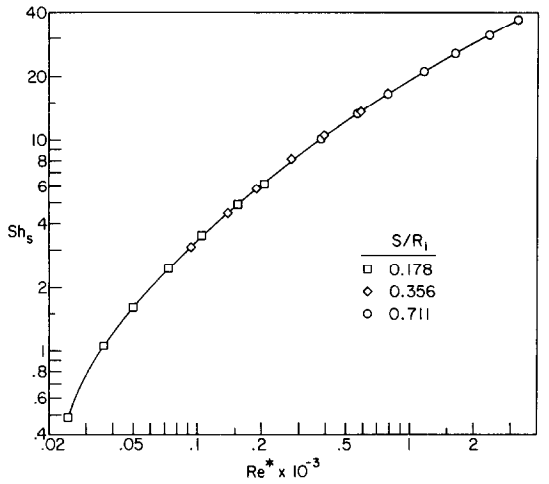

FIG. 6. Universal Sherwood number–Reynolds number correlation.

To use the Sh_s, Re^* correlation to determine the Sherwood number for any S/R_i between 0.178 and 0.711, a functional relationship for $\lambda = \lambda(S/R_i)$ must be available. The following linear function was found by least squares to best fit the three available λ values

$$\lambda = -1.8588 + 4.0047(S/R_i). \quad (8)$$

To predict the Sherwood number for given values of S/R_i and ω, the appropriate steps are to compute λ from equation (8), R^* from equation (5), and Re^* from equation (6). Then, Sh_s can be read directly from Fig. 6 using Re^* as input. To facilitate more accurate predictions than are possible using the grid-free, journal version of Fig. 6, the coordinates of the universal Sh_s, Re^* distribution are listed in Table 1 to facilitate its replotting on graph paper.

To demonstrate the validity of the universal correlation, it was used to predict the Sh_i, R_i/S distributions of Fig. 4. These predictions are plotted as dashed lines in the figure. As seen there, the predicted Sh_i are of satisfactory accuracy. Overall, the average errors are about 2%, with an extreme error of $6\frac{1}{2}$%. At the larger spacings, the predictions are error free.

Table 1. Coordinates of Fig. 6

Re^*	Sh_s	Re^*	Sh_s	Re^*	Sh_s
25	0.50	90	3.02	600	13.8
30	0.77	100	3.35	800	16.6
35	1.01	120	3.96	1000	19.1
40	1.23	140	4.52	1200	21.2
45	1.44	160	5.08	1400	23.2
50	1.64	180	5.62	1600	25.0
55	1.83	200	6.12	2000	28.1
60	2.00	250	7.36	2500	31.8
70	2.36	300	8.44	3000	35.1
80	2.70	400	10.5	3200	36.3

Literature comparisons

As noted in the Introduction, no prior information was encountered on rotating annular fins, thereby precluding direct comparison of the present results with the literature. In considering other rotating bodies with which to make comparisons, it appears that the unfinned rotating shaft and the rotating disk are the most relevant.

The fluid flow and heat (mass) transfer for a rotating disk are an exact solution of the governing conservation equations. The mass transfer coefficient predicted by theory [2] for naphthalene sublimation at a rotating disk is

$$K/\mathscr{D} = 0.884(\omega/2\nu)^{1/2}. \quad (9)$$

According to theory, the local transfer coefficient is uniform over the disk surface, so that the local and average coefficients are equal. Naphthalene sublimation experiments for a rotating disk [3], performed with a test setup similar to that employed here, yielded mass transfer coefficients which agreed to within a few percent with those of equation (9).

Heat transfer results for unfinned rotating shafts are reported in the literature and, in addition, unpublished naphthalene sublimation experiments have been performed at Minnesota. Those experiments were contemporaneous with those reported here, used a similar apparatus, and were carried out with a virtually identical experimental technique. In view of these factors, the just-cited naphthalene sublimation results for the unfinned rotating shaft will be used for comparison with the present annular fin results, in preference to literature information on rotating-shaft heat transfer.

The comparisons are made in Fig. 3, where the present results are plotted in the Sh_i, Re_i format. The results for the rotating disk can be recast into this format by multiplying through equation (9) by D_i, yielding

$$Sh_i = 0.884\, Re_i^{1/2}. \quad (10)$$

This equation is plotted as the short-dashed straight line in Fig. 3. The data for the unfinned rotating shaft (diameter D_i) are represented by the long-dashed line.

From the figure, it is seen that, broadly speaking, the Sherwood number values for the fins, the disk, and the unfinned shaft fall in the same general range. The disk Sherwood numbers are greater than those for the most closely spaced fins and, at lower Reynolds numbers, also exceed those for the next-to-closest spaced fins. On the other hand, the Sherwood numbers for the more widely spaced fins are larger than the disk values over the entire investigated range of Re_i.

At Reynolds numbers beyond the investigated range, the disk results fall below those for all of the interfin spacings. Thus, for these larger Reynolds numbers, the disk results serve as a lower bound for the fin results and, if used in design, would yield a conservative prediction of the rate of heat (mass) transfer from the fins.

The Sherwood numbers for the unfinned rotating shaft are generally lower than those for the fins, except for the smallest interfin spacing and at lower Re_i. The fact that the fin transfer coefficients are usually larger than those for the unfinned shaft provides an incentive for the use of fins.

CONCLUDING REMARKS

The experimental work reported here yielded mass transfer coefficients for an array of shaft-attached, rotating annular fins. The Sherwood numbers for mass transfer can be converted to Nusselt numbers for heat transfer by the relation $Nu = Sh(Pr/Sc)^n$ where, for most convective heat (or mass) transfer situations, n is in the range between 1/3 and 0.4 (note that $Sc = 2.5$ for naphthalene sublimation in air). The measured Sherwood numbers correspond to Nusselt numbers for fins whose efficiency is equal to unity. It appears that heat transfer coefficients for shaft-attached, rotating annular fins have heretofore been unavailable in the heat transfer literature.

Primary attention was focused on the response of the fin transfer coefficient to variations of the interfin spacing and the rotational speed. The former, expressed as the ratio S/R_i (S = interfin spacing, R_i = radius of shaft), ranged from 0.178 to ∞. The latter, when expressed in terms of a Reynolds number based on the shaft surface speed and the shaft diameter, extended from 700 to 6000. The radius ratio of the annular fin was fixed at 1.55.

The fin mass (heat) transfer coefficient decreased with decreasing fin spacing, with the extent of the decrease being highly sensitive to the rotational speed (i.e. to the Reynolds number). At the lowest investigated Reynolds number, the overall spacing-related decrease of the coefficient was a factor of six, while at the highest Reynolds number the decrease was only about 35%. Thus, from the standpoint of design, closely spaced fins can be used at higher Reynolds numbers without a significant spacing-related decrease in the transfer coefficient. On the other hand, at low Reynolds numbers, the fins must be spaced farther apart to avoid overly low values of the coefficient.

The variation of the transfer coefficient with rotational speed was quite sensitive to the interfin spacing. In particular, at very small spacings, the coefficient dropped off very rapidly as the Reynolds number decreased in the range of low Reynolds numbers.

To facilitate the use of the experimental results for design, a correlation was developed which represents the Sherwood number as a continuous function of the investigated independent variables of the problem.

The annular-fin Sherwood numbers were compared with those for a rotating disk and for an unfinned rotating shaft. For the most part, the fin Sherwood numbers substantially exceeded the unfinned-shaft Sherwood numbers, thereby providing an incentive for finning. The fin and disk Sherwood numbers intermingled at lower and intermediate Reynolds numbers, but at Reynolds numbers beyond those considered here, the disk Sherwood numbers fall below those for the fins.

Supplementary experiments demonstrated that the measured Sherwood numbers were unaffected by natural convection, even at the lowest investigated Reynolds number.

REFERENCES

1. F. Kreith, Convective heat transfer in rotating systems. In *Advances in Heat Transfer*, Vol. 5, pp. 129–251 (1968).
2. E. M. Sparrow and J. L. Gregg, Heat transfer from a rotating disk to fluids of any Prandtl number, *Trans. Am. Soc. mech. Engrs*, Series C, *J. Heat Transfer* **81**, 249–251 (1959).
3. S. Palsdottir, Heat transfer at and adjacent to the tip of a rotating cylinder. M.S. thesis, Department of Mechanical Engineering, University of Minnesota, Minneapolis, MN (1981).

TRANSFERT THERMIQUE PAR DES AILETTES ANGULAIRES TOURNANTES

Résumé—Des expériences sont conduites pour déterminer les coefficients de transfert thermique par des arrangements d'ailettes annulaires sur un arbre tournant. Elles concernent un grand domaine de vitesse de rotation et d'espaces entre ailettes (incluant le cas limite d'une seule ailette annulaire). L'efficacité des ailettes était égale à l'unité. On trouve que le coefficient de transfert thermique d'ailette décroît quand l'espace entre ailettes diminue, avec l'étendue de la décroissance qui est importante aux faibles vitesses de rotation, mais modérée aux grandes vitesses. Ainsi des ailettes serrées peuvent être utilisées aux fortes vitesses de rotation, sans décroissement du coefficient de transfert significativement lié à l'espacement, mais aux faibles vitesses les ailettes doivent être suffisamment séparées pour éviter des valeurs basses du coefficient. Celui-ci décroît aussi quand la vitesse de rotation diminue, avec une chute particulièrement rapide aux faibles vitesses quand l'espacement des ailettes est petit. La plupart du temps les coefficients de transfert thermique de l'ailette dépassent notablement ceux de l'arbre tournant non aileté. On trouve aussi qu'aux grandes vitesses de rotation, le coefficient de transfert pour un disque tournant est une limite inférieure pour le cas des ailettes annulaires. Pour faciliter l'utilisation dans les cas pratiques, une formule est donnée qui représente le coefficient de transfert d'ailette comme une fonction continue des paramètres indépendants étudiés.

WÄRMEÜBERGANG AN ROTIERENDEN KREISRIPPEN

Zusammenfassung—Es wurden Experimente zur Bestimmung des Wärmeübergangskoeffizienten an Reihen von kreisringförmigen Rippen, die auf einer rotierenden Welle angebracht waren, durchgeführt. Die Untersuchungen umfassen einen großen Bereich von Drehgeschwindigkeiten und Rippenabständen (auch den Grenzfall der einzelnen ringförmigen Rippe). Der Rippenwirkungsgrad war gleich eins. Es ergab sich, daß der Wärmeübergangskoeffizient an den Rippen mit kleiner werdendem Rippenabstand abnimmt, wobei die Abnahme bei kleinen Drehgeschwindigkeiten ausgeprägt aber bei großen Geschwindigkeiten nur gemäßigt vorhanden ist. Demgemäß ist bei dicht angeordneten Rippen und großen Drehgeschwindigkeiten keine vom Abstand der Rippen abhängige, signifikante Abnahme der Wärmeübergangskoeffizienten vorhanden. Bei kleinen Drehgeschwindigkeiten müssen die Rippen mit großem Abstand angeordnet werden, um zu kleine Koeffizienten zu vermeiden. Der Wärmeübergangskoeffizient nimmt mit abnehmender Drehgeschwindigkeit ebenfalls ab, wobei ein besonders rascher Abfall bei kleinen Geschwindigkeiten und kleinem Rippenabstand vorhanden ist. Die Wärmeübergangskoeffizienten an der berippten Welle sind in der Regel wesentlich größer als an einer unberippten. Eine Berippung empfiehlt sich also. Weiterhin wurde herausgefunden, daß bei hohen Drehgeschwindigkeiten der Wärmeübergangskoeffizient für eine rotierende Scheibe als untere Grenze für ringförmige Rippen angesehen werden kann. Zur leichteren Anwendung der Ergebnisse für die Auslegung wurde eine Beziehung entwickelt, welche den Wärmeübergangskoeffizienten an den Rippen als kontinuierliche Funktion der untersuchten unabhängigen Parameter beschreibt.

ТЕПЛОПЕРЕНОС ОТ ВРАЩАЮЩИХСЯ КОЛЬЦЕВЫХ РЕБЕР

Аннотация—Проведены эксперименты по определению коэффициентов теплообмена для рядов вращающихся кольцевых ребер, прикрепленных к валу. Эксперименты охватывают широкий диапазон скоростей вращения и межреберных расстояний (включая предельный случай единичного ребра). Эффективность ребер равна единице. Найдено, что коэффициент теплообмена ребра падает с уменьшением межреберного расстояния, причем при малых скоростях вращения падение достигает наибольших значений, а при больших—является умеренным. Таким образом, близко расположенные ребра могут использоваться при больших скоростях вращения без существенного влияния межреберного расстояния на коэффициент теплообмена, тогда как при малых скоростях во избежание сильного уменьшения коэффициента межреберные расстояния должны быть большими. Коэффициент теплообмена падает с уменьшением скорости вращения, причем при малых скоростях и межреберных расстояниях падение резкое. Большей частью коэффициенты теплообмена оребренного вала выше, чем для неоребренного, что указывает на эффективность оребрения. При больших скоростях вращения коэффициент теплообмена для вращающегося диска служит нижней границей коэффициентов теплообмена кольцевого ребра. Для расчетных целей выведено соотношение, представляющее коэффициент теплообмена ребра как функцию независимых параметров.